*Geophysical Research Letters*

Supporting Information for

# Investigating Diurnal and Seasonal Cycles of Vegetation Optical Depth Retrieved from GNSS Signals in a Broadleaf Forest

Yitong Yao[1], Vincent Humphrey[2,3], Alexandra G. Konings[4], Yujie Wang[1], Yi Yin[5], Nataniel Holtzman[4], Jeffrey D. Wood[6], Yinon Bar-On[1], Christian Frankenberg[1,7]

[1] Division of Geological and Planetary Sciences, California Institute of Technology, Pasadena, CA 91125, USA

[2] Department of Geography, University of Zürich, Zürich, Switzerland

[3] Federal Office of Meteorology and Climatology MeteoSwiss, Zürich, Switzerland

[4] Department of Earth System Science, Stanford University, Stanford, CA 94305, USA

[5] Department of Environmental Studies, New York University, NY 10012, USA

[6] School of Natural Resources, University of Missouri, Columbia, MO 65211, USA

[7] Jet Propulsion Laboratory, California Institute of Technology, Pasadena, CA 91109, USA

**Contents of this file**

**Text S1**

Vector Autoregression (VAR) serves as the predictive regression method in this study, aiming to quantify the lagged linear relationship between multiple variables as they change over time. The variables included in the VAR analysis are VOD, soil moisture content (SMC), diurnal temperature amplitude (dT), and leaf area index (LAI) at daily scale. Here dT is known to be directly related to land surface energy fluxes (Feldman et al., 2022; Panwar et al., 2019). As dT is still coupled to short-wave solar radiation (Rad) at daily scale, we did not include Rad in the VAR model. Prior to employing VAR, Augmented Dicky-Fuller tests confirmed the stationarity of these variables, a prerequisite for VAR approaches. Specifically focusing on VOD, the VAR model effectively captures the dynamics throughout the study period with $R^2$ value of 0.65 when the lag order is 1. Regression constants and slope vectors were solved using ordinary least squares. The influence of multiple variables on VOD was quantified using Eq. (S1-S3) following Feldman et al (2020).

$$Y_t = \alpha + \sum_p \beta_p Y_{t-p} + e_t \quad \text{Eq. (S1)}$$

$$Y_t = [VOD_t, SMC_t, dT_t, LAI_t]' \quad \text{Eq. (S2)}$$

$$\frac{\Delta VOD}{\Delta t}_{X_{t-1} \to VOD_t} = \frac{\partial X}{\partial t} \beta_{X_{t-1} \to VOD_t} \quad \text{Eq. (S3)}$$

Where $\alpha$ and $\beta$ are the regression constant and slope vectors. $e_t$ are the residuals. p is the lag order. Here, p=1. Eq. (S1) was solved using ordinary least squares.

As shown in Figure S1, soil moisture primarily drove VOD variations, while an increase in dT contributed to a decrease in plant water content. The influence of dT was not found to be significant. Leaf shedding denoted by LAI decrease during dry downs also resulted in a drop in VOD, as confirmed by positive coefficient from $LAI_{t-1}$ to $VOD_t$.

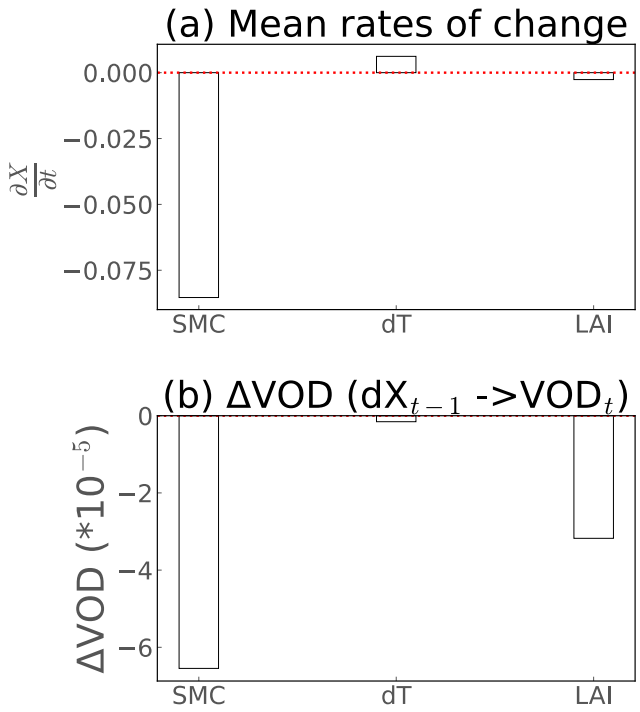


Figure S1 (a) Mean rates of change during the growing season in soil moisture (SMC), diurnal temperature amplitude (dT), and leaf area index (LAI) during drydown periods. The average of day-to-day difference in SMC, dT and LAI is shown. The red line is the zero line. (b) Change in VOD due to changes in SMC, dT, and LAI as calculated by Eq. (S3). Here, ΔVOD driven by each term is the product of β from VAR model and $\frac{\partial X}{\partial t}$ in panel (a).

**Text S2**

A non-steady-state plant hydraulics scheme models water flow, water storage, and water potential within the plant. This involves a system of ordinary differential equations representing water flow between each leaf, branch, trunk, and root (Holtzman et al., 2023). VOD is parameterized as a function of $\psi_{leaf}$ and LAI. These unknown parameters were retrieved directly using microwave brightness temperatures at a nearby location with a more homogeneously forested area since MOFLUX site is a mix of forest and cropland. The Tau-omega zeroth-order radiative transfer model was used, simulating brightness temperature as a function of the soil surface dielectric constant and VOD.

Following the retrieval of unknown parameters, the CliMA-Land model can simulate VOD at an hourly scale. Consequently, comparisons between modeled VOD and GNSS VOD can be conducted at both seasonal and diurnal scales.

**Text S3**

The GNSS technique provides angular heterogeneity due to varying incidence angles and azimuth angles. The inclination of the receiving signals corresponding to navigation satellites varies throughout the day, resulting in a footprint of GNSS VOD that spans dozens to hundreds of meters depending on the elevation angle ($r=h/\tan(10^o)$, h is canopy height and r is the radius. $10^o$ is the minimum elevation angle that is taken into account), which is a footprint that is roughly comparable to eddy-covariance flux towers. For example, average canopy height at US-MOz is about 17-20 m, therefore the resulting circle radius is 96-113 m.

We recognize that GNSS SNR measurements might be influenced by volume scattering and indirect ground multipath reflections. The successive constructive and destructive interference from ground reflections causes a periodic oscillation of the SNR, which is a function of incidence angle. However, these periodic oscillations are found to be about an order of magnitude smaller than the canopy water attenuation in the line of sight (Humphrey & Frankenberg, 2023). Moreover, observations with an incidence angle higher than $80^o$ have been excluded to eliminate co-polarized GNSS signals.

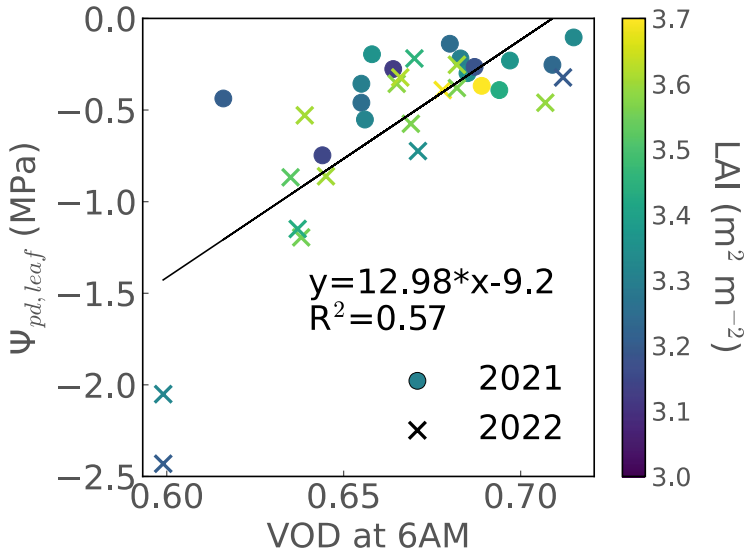


Figure S2 The relationship between community predawn leaf water potential ($\psi_{pd,leaf}$) and VOD at 6AM for the year 2021 and 2022. Only measurements made during the stable LAI period (LAI > 3.0 $m^2$ $m^{-2}$) were used. Measurements made on rainy days have been removed.

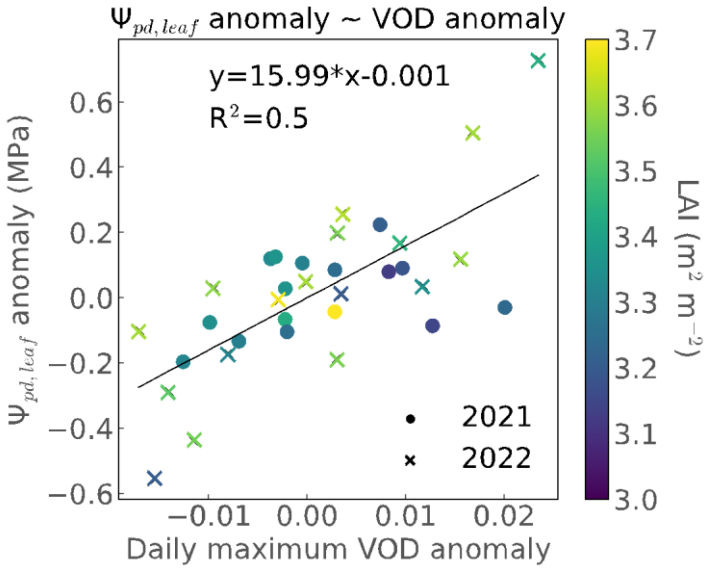


Figure S3 The relationship between daily anomaly of VOD and anomaly of $\psi_{pd,leaf}$.

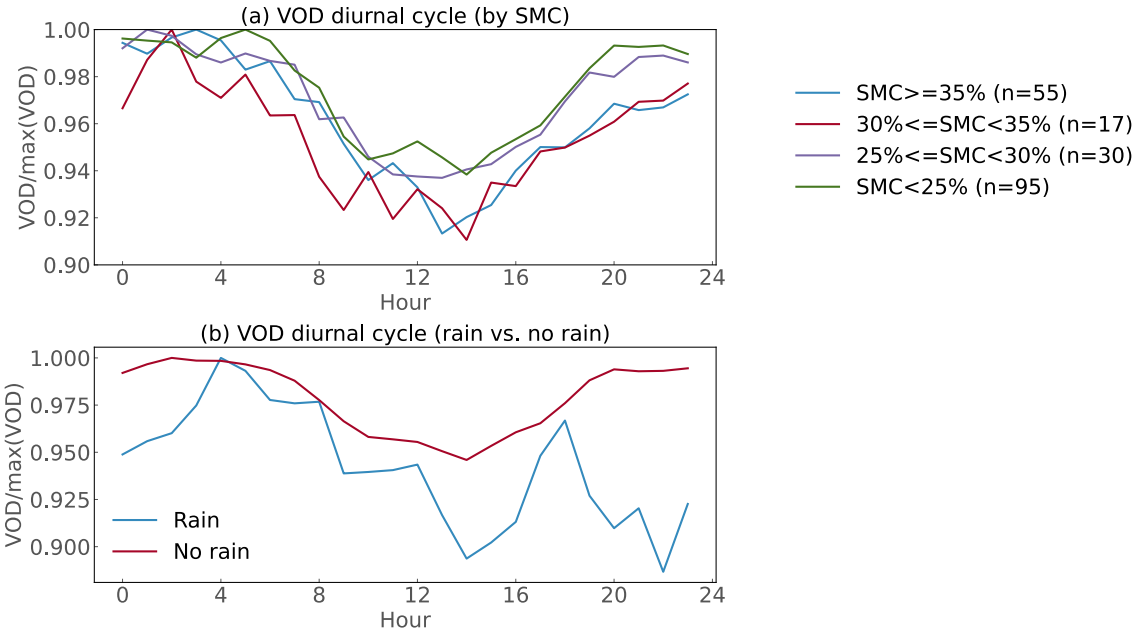


Figure S4 Average diurnal cycle of normalized VOD (by their maximum) grouped by (a) varying water stress conditions denoted by SMC, (b) rainfall events. Only measurements made during the stable LAI period (LAI > 3.0 $m^2$ $m^{-2}$) were used.

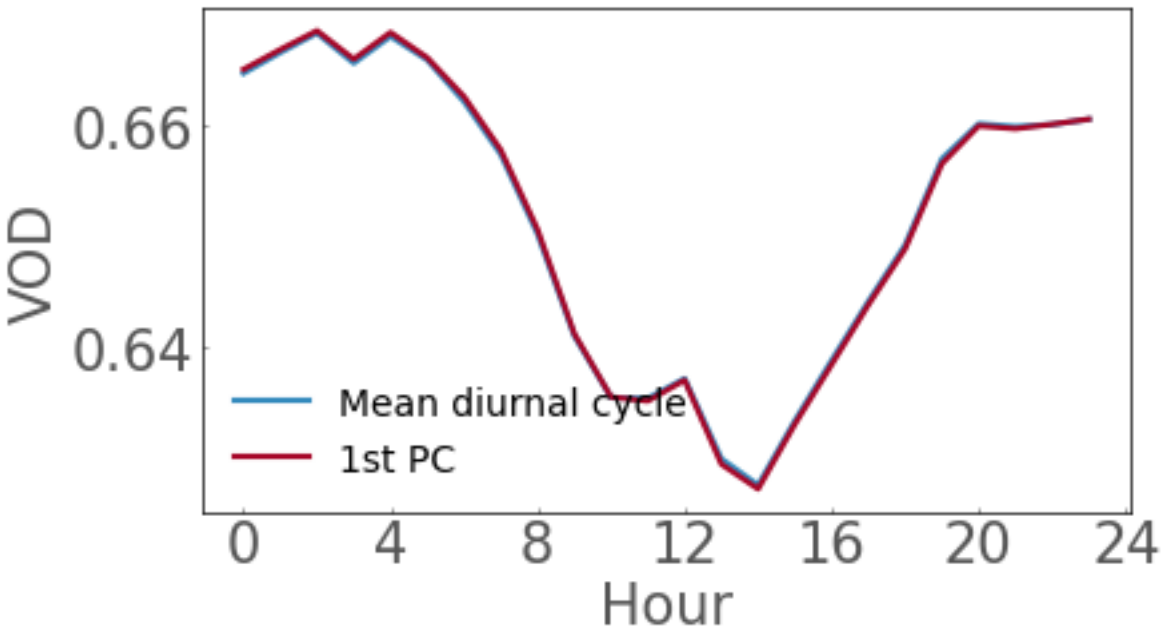


Figure S5 The mean diurnal cycle and 1st PC of GNSS VOD. These two lines almost overlap. All measurements on rainy days were removed.

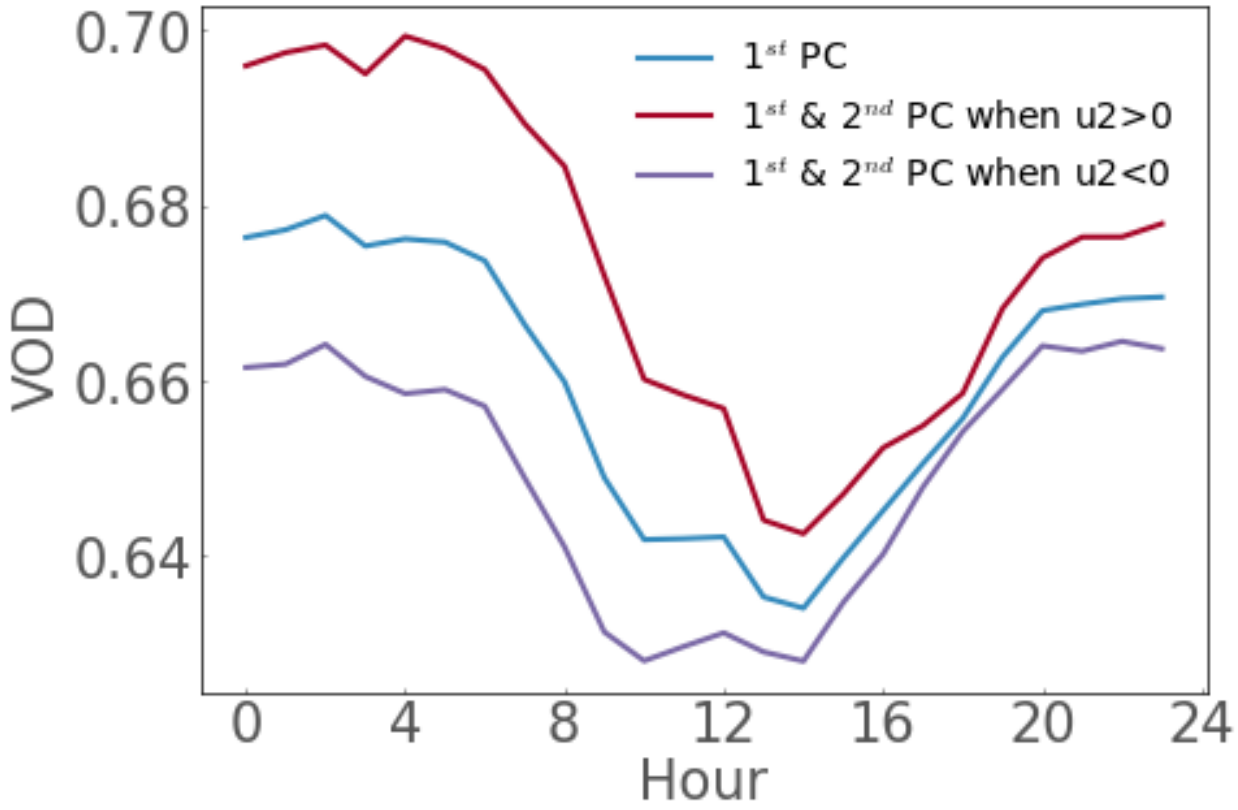


Figure S6 The reconstruction of GNSS VOD diurnal cycle using VOD principal components.

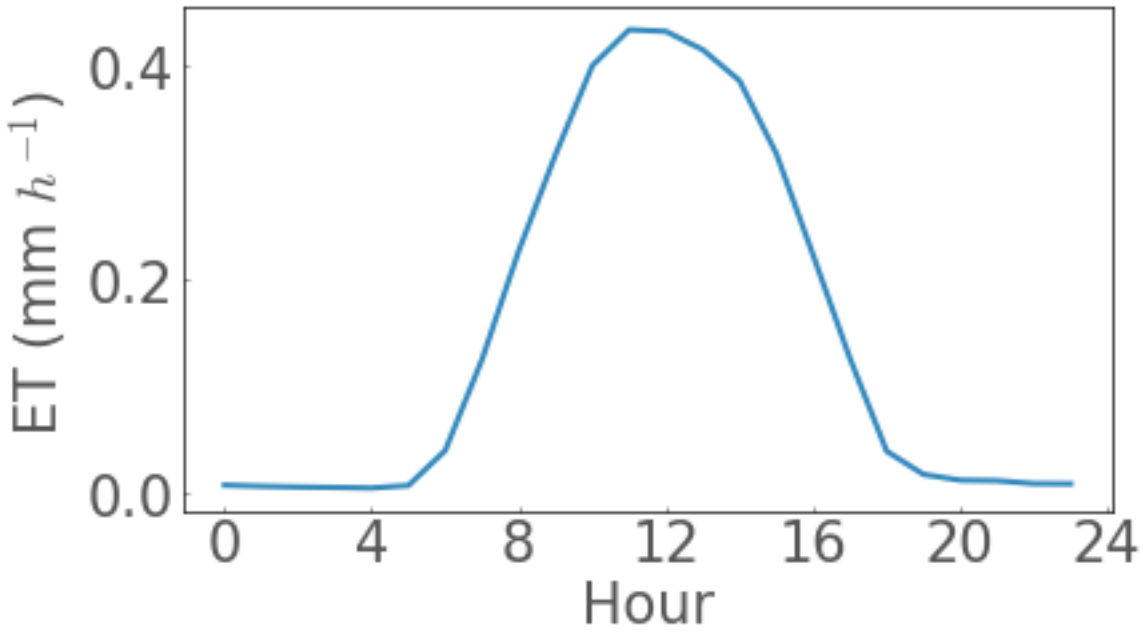


Figure S7 The mean diurnal cycle of observed ET.

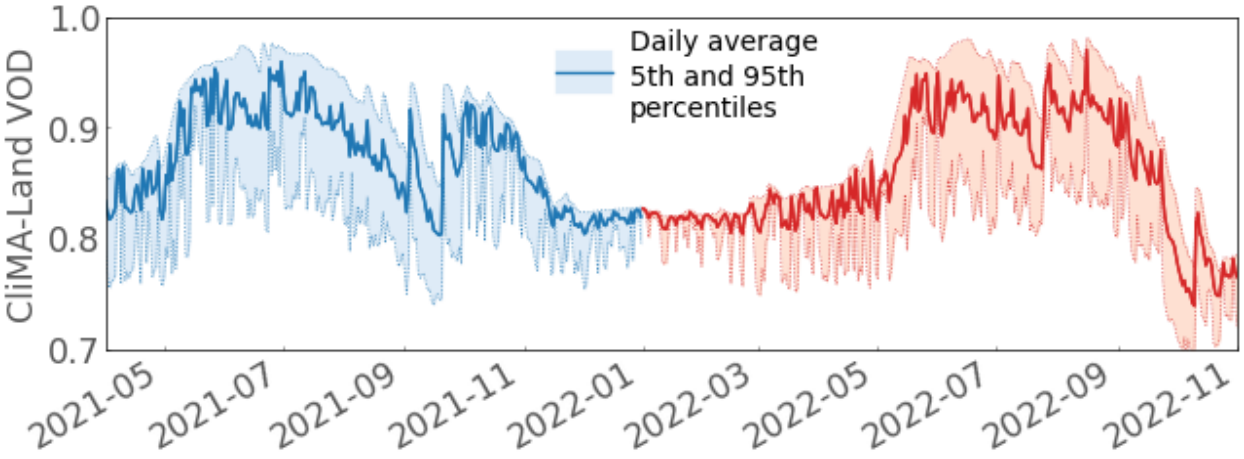


Figure S8 The time series of VOD simulated by the CliMA-Land model.

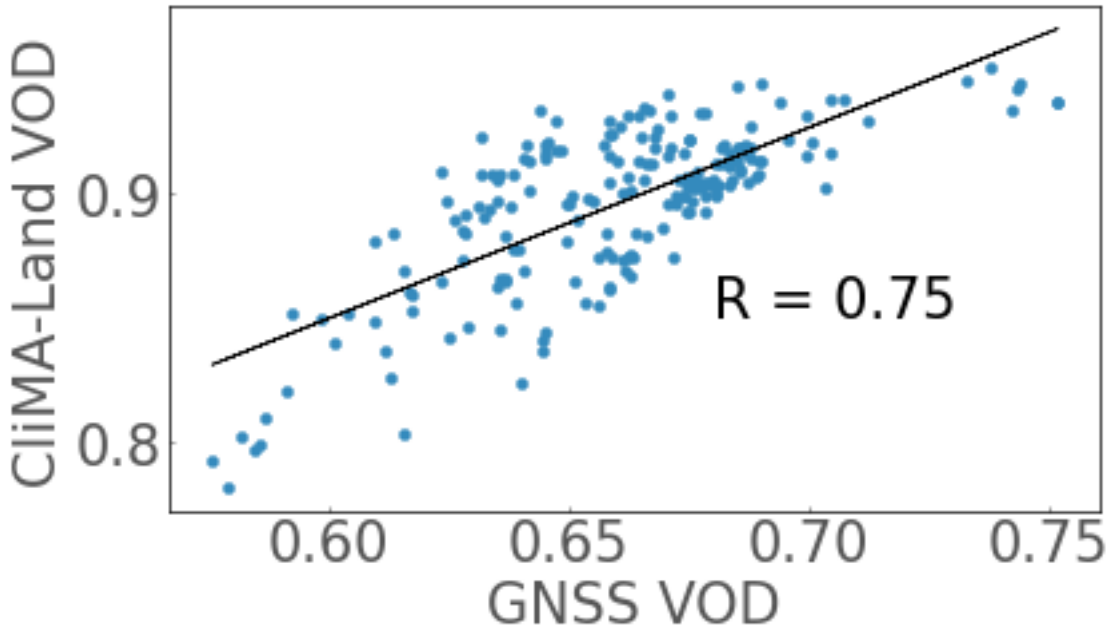


Figure S9 CliMA-Land VOD versus GNSS VOD at daily scale.

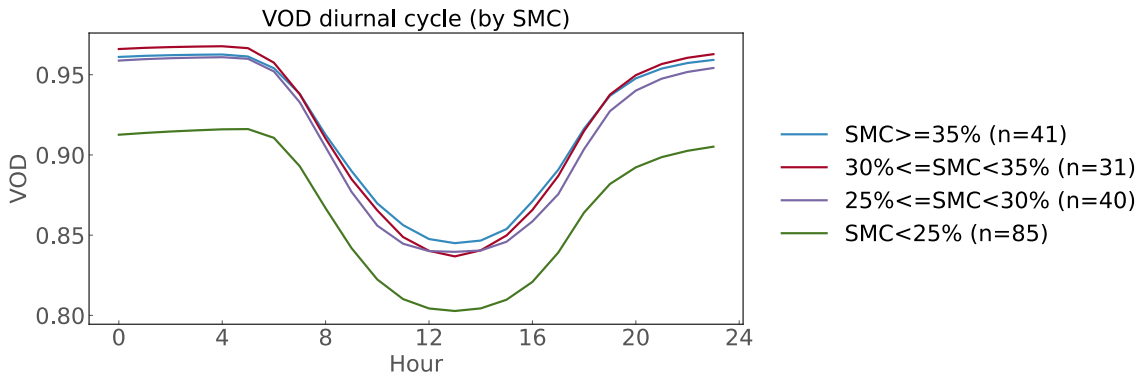


Figure S10 Average diurnal cycle of CliMA-Land VOD grouped by varying water stress conditions denoted by SMC. Here SMC is daily average.

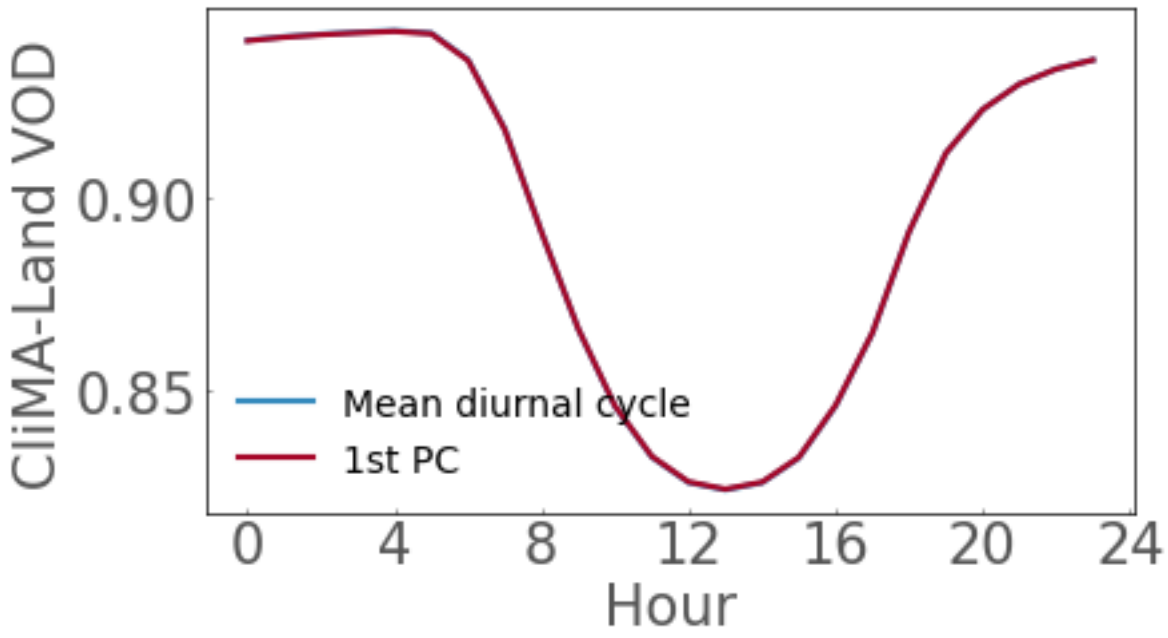


Figure S11 The mean diurnal cycle and 1st PC of CliMA-Land VOD. These two lines almost overlap. All measurements on rainy days were removed.

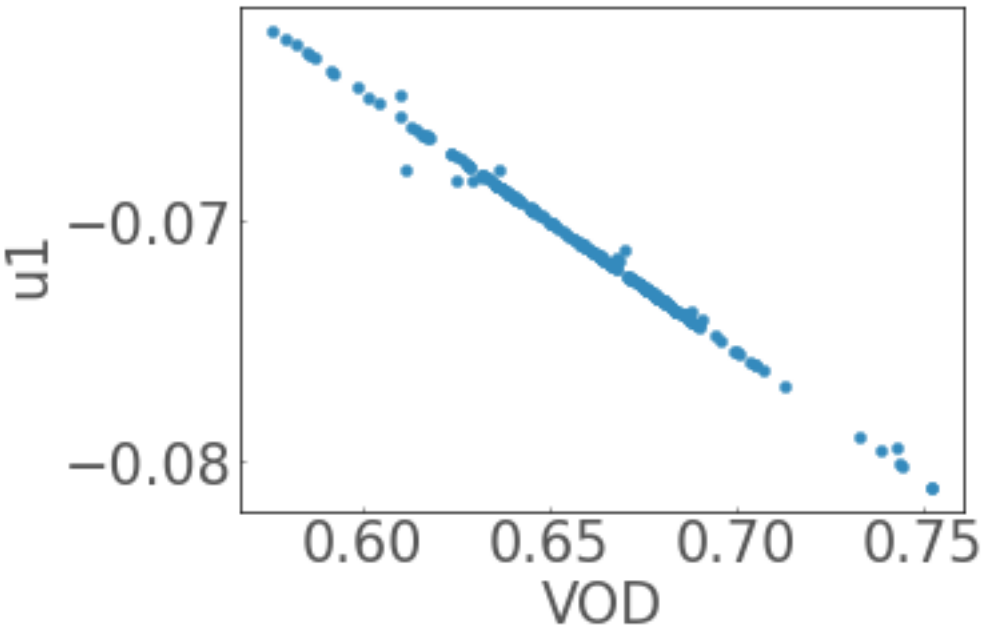


Figure S12 The relationship between temporal loadings of 1st PC and VOD magnitude.